

Stochastic Fluctuations in Epidemics on Networks

M. Simões, M. M. Telo da Gama and A. Nunes *

*Centro de Física Teórica e Computacional and Departamento de Física,
Faculdade de Ciências da Universidade de Lisboa,
P-1649-003 Lisboa Codex, Portugal*

Abstract

The effects of demographic stochasticity in the long term behaviour of endemic infectious diseases have been considered for long as a necessary addition to an underlying deterministic theory. The latter would explain the regular behaviour of recurrent epidemics, and the former the superimposed noise of observed incidence patterns. Recently, a stochastic theory based on a mechanism of resonance with internal noise has shifted the role of stochasticity closer to the center stage, by showing that the major dynamic patterns found in the incidence data can be explained as resonant fluctuations, whose behaviour is largely independent of the amplitude of seasonal forcing, and by contrast very sensitive to the basic epidemiological parameters. Here we elaborate on that approach, by adding an ingredient which is missing in standard epidemic models, the 'mixing network' through which infection may propagate. We find that spatial correlations have a major effect in the enhancement of the amplitude and the coherence of the resonant stochastic fluctuations, providing the ordered patterns of recurrent epidemics, whose period may differ significantly from that of the small oscillations around the deterministic equilibrium. We also show that the inclusion of a more realistic, time correlated, recovery profile instead of exponentially distributed infectious periods may, even in the random-mixing limit, contribute to the same effect.

PACS numbers: 89.75.-k, 87.10.+c, 87.23.-n

* corresponding author
anunes@ptmat.fc.ul.pt

I. INTRODUCTION

The incidence patterns of childhood diseases in the twentieth century have been a challenge and a preferred testing ground for epidemiological models. During the last decade, more sophisticated approaches building on the traditional SIR and SEIR models [1] (see Section II for a description) have brought considerable advances in understanding and selecting some of the fundamental ingredients of the complex dynamics of infectious diseases ([2], [3], [4]). The interplay between the system's nonlinearity and the periodic perturbation in seasonally forced SIR and SEIR models was shown to be a source of complex dynamics compatible with the diversity of observed incidence records ([5], [6], [7]).

This body of work belongs to an essentially deterministic framework, where demographic stochasticity plays a secondary role, except when addressing stochastic extinction ([8],[9]). In this framework, the role of stochasticity is that of sustaining small amplitude oscillations around the deterministic system's equilibrium that follow the natural frequency given by the local linear approximation ([6], [10], [11]), or else that of promoting the switching between different competing attractors of the underlying deterministic model ([12],[13]).

Recently, a stochastic theory developed for a predator-prey competition model [14] and then applied to the well-mixed SIR model [15] has shown that the fluctuation power spectrum of the incidence time series is essentially determined, both in the presence and in the absence of seasonal forcing, by the resonance with internal noise of the system's natural frequency in the deterministic (infinite population size) limit. The cross correlation structure of this internal noise can be computed analytically from the transition probabilities, and it may shift the resonance peak away from the system's natural frequency. The amplitude and the coherence of these resonant fluctuations are both large for the parameter values that correspond to some childhood diseases, so that they may be comparable even in large systems to the oscillations induced by seasonal forcing.

Apart from stochasticity, another missing ingredient of the standard epidemic models that has been attracting increasing attention is the host population contact structure, or 'mixing network' [16], [17]. Most of the research connecting networks and epidemiology

dates from the last five years, when many fundamental results of network theory became widely known while new ones have been derived [18], [19], [20]. These ideas originated in the mathematics and physics communities were applied in an epidemiological setting from the beginning [21], [22], [23] prompting the interest of epidemiologists and several theoretical [24], [25], [26] and field epidemiology [27], [28], [29] results.

Here we address the effect of relaxing the random mixing assumption on the behaviour of the resonant fluctuations of a stochastic SIR model. We assume that the host population contact network may be represented by a 'small-world' network of the type introduced by Watts and Strogatz nearly a decade ago [21]. Analysis of real networks of social contacts [30] indicates that this is a reasonable first assumption to model the contact structure relevant for the propagation of airborne infections. We find that spatial correlations have a major effect in the enhancement of the amplitude and of the coherence of the resonant stochastic fluctuations, providing ordered patterns of recurrent epidemics. The shift of the resonance peak away from the system's natural frequency also increases significantly due to correlations. The enhanced amplitude and coherence of the fluctuations implies that in populations where a disease spreads predominantly through local infectious contacts, large epidemic outbursts with well defined recurrence times are generated by internal noise alone, without the presence of seasonal forcing. This effect is illustrated in Section II.B with a particular example, and studied systematically in Section III.B.

Another assumption of the SIR model which has been challenged [31], [32], [33] is that of considering a constant recovery probability during the infection period. We study the effect on the resonant fluctuations of switching from the (uncorrelated) exponentially distributed infection periods used in [15] to the opposite limit of (time correlated) constant infection periods. Again, we find that the spectrum of stochastic fluctuations found in [15] changes under more realistic assumptions on the recovery profile in such a way that the oscillations become larger and more sharply defined. In this case, the peak frequency shift with respect to the deterministic prediction is larger, and towards larger frequencies.

Qualitatively, the effects of spatial and time correlations on the fluctuation spectrum are

similar: both the spatial correlations, introduced through the host population contact network, and the time correlations, introduced via constant infection periods, lead to enhanced more sharply defined dominant peaks. There are analogues of this behaviour in many systems studied in statistical physics. The peak frequency shift, however, is more pronounced and has a different sign for the model with constant infection period. As discussed in Sections II.B and III.C, this qualitative difference can be understood on the basis of an effective deterministic description.

These results show that the classical understanding of the incidence time patterns of endemic infectious diseases, which is mainly based on a seasonally forced deterministic description, is clearly insufficient to have a correct description of such fluctuations. These may be purely stochastic, and the diversity of incidence patterns found in real data for the same disease in different populations can be understood in this framework as an effect of population size and contact structure.

Moreover, the approximate period of the recurrent epidemics driven by internal noise in the presence of spatial and/or time correlations differs significantly from the period computed in the usual deterministic approach. This is an important cautionary note with regard to the use, in the framework of the deterministic description, of the recurrence period to help assess estimates of epidemiological parameters. The breakdown of the assumptions of random mixing of the population and/or of constant recovery rate during the infectious period implies important corrections to the dominant frequency of the fluctuations.

II. METHODS

A. Susceptible-Infectious-Recovered (SIR) dynamics in a randomly mixed discrete population

One of the simplest epidemiological models one can consider is based on dividing the whole population in three classes of individuals, the susceptible, the infectious, and the permanently recovered. It is suitable to study the infection dynamics of diseases that confer

long lasting immunity, such as childhood infections, provided that we take into account in the long term dynamics the replenishment of susceptibles in the population through births.

The deterministic description of the basic Susceptible-Infectious-Recovered (SIR) model in a closed population where renewal of susceptibles occurs through births with a constant birth rate and death rate μ is given by the equations

$$\begin{aligned}\dot{s} &= \mu(1 - s) - \beta si \\ \dot{i} &= \beta si - (\gamma + \mu)i\end{aligned}\tag{1}$$

where s , i are the densities of susceptible and infectious individuals, respectively, γ the recovery rate of the disease and β its transmissibility. A crucial parameter for the behaviour of this model is the so called basic reproductive rate, $R_0 = \beta/(\gamma + \mu)$. For $R_0 < 1$ the disease dies out, while for $R_0 > 1$, the disease is endemic in the population. In this case, system (1) has a non trivial endemic equilibrium at $s^* = (\gamma + \mu)/\beta$, $i^* = (\mu/\beta)(1/s^* - 1)$, and the small oscillations around this equilibrium have damping factor $-\mu/(2s^*)$ and period $2\pi/(\sqrt{\mu\beta(1 - s^*) - (\mu/2s^*)^2})$. The Susceptible-Exposed-Infectious-Recovered (SEIR) model considers an additional class of infected, but not yet infectious, individuals.

In a randomly mixed discrete population of N individuals, SIR dynamics may be described as a continuous time Markov process on a population divided into three classes, susceptibles, infectious and recovered. The state of the system is characterized by the numbers S , I and $R = N - S - I$, of individuals in each of the three classes, and the events of infection, death, birth and recovery correspond to the following transitions and transition rates

$$\begin{aligned}T[(S, I) \rightarrow (S - 1, I + 1)] &= \beta SI/N \quad \text{infection} \\ T[(S, I) \rightarrow (S - 1, I)] &= \mu S \quad \text{death of a susceptible} \\ T[(S, I) \rightarrow (S, I - 1)] &= \mu I \quad \text{death of an infectious} \\ T[(S, I) \rightarrow (S, I)] &= \mu(N - S - I) \quad \text{death of a recovered} \\ T[(S, I) \rightarrow (S + 1, I)] &= \mu N \quad \text{birth} \\ T[(S, I) \rightarrow (S, I - 1)] &= \gamma I \quad \text{recovery,}\end{aligned}\tag{2}$$

where $(S, I) \rightarrow (S', I')$ denotes the transition from state (S, I) to state (S', I') and $T[(S, I) \rightarrow (S', I')]$ the corresponding transition rate.

As detailed in [15], a good approximation for the power spectrum of the stochastic fluctuations around the stationary population numbers can be computed analytically from the linear Fokker-Planck equation obtained from the next to leading order terms in van Kampen's expansion of the master equation associated to (2). The leading order terms of the expansion yield the deterministic equations (1), that describe the behaviour of the system in the limit of infinite populations.

Following this approach, we have computed the power densities P_S and P_I of the fluctuations of susceptibles and infectious individuals for process (2), scaled by the square root of the system size \sqrt{N} , as a function of the angular frequency ω ,

$$\begin{aligned} P_S(\omega) &= 2\mu \left(1 - \frac{\gamma + \mu}{\beta}\right) \frac{(\gamma + \mu)^2 + \omega^2}{(\omega^2 - D)^2 + (T\omega)^2} \\ P_I(\omega) &= 2\mu \left(1 - \frac{\gamma + \mu}{\beta}\right) \frac{\omega^2 + \mu^2(1 - \beta/(\gamma + \mu) + (\beta/(\gamma + \mu))^2)}{(\omega^2 - D)^2 + (T\omega)^2} \end{aligned} \quad (3)$$

where $D = \mu(\beta - \gamma - \mu)$ and $T = -\beta\mu/(\gamma + \mu) = -R_0\mu$, denoting as before by R_0 the basic reproductive rate of the disease. The parameters D and T are equal to the determinant and to the trace, respectively, of the linear approximation of (1) at the endemic equilibrium, and they have a simple dynamical interpretation: D is the square of the frequency of the small oscillations around the equilibrium when the damping is small, and T is twice the damping factor of these oscillations.

Equations (3) are independent of N because the dependence of the amplitude of the fluctuations on system size has been scaled out, and they describe exactly the stochastic process (2) in the limit of large N . These power spectra are resonant like, showing that the amplitude of the fluctuations as a function of their time scale is governed by a mechanism of resonance of internal noise with the system's natural frequency \sqrt{D} . The resonance peak will be shifted away from \sqrt{D} , depending on the values of T and on the terms in the numerator of (3), which are determined by the cross correlation structure of the internal noise. However,

when T is small, the shift in the resonance peak with respect to \sqrt{D} is also small.

The relevance and universality of this type of 'endogenous' stochastic resonance for ecological systems in general was first argued in [14]. The complete analytic description of the phenomenon given in [14], [15] relies on the random mixing assumption and on the constant recovery rate assumption. The effect of relaxing these assumptions, crucial in more realistic settings, must be tested through stochastic simulations.

B. The SIR model on dynamic small-world networks

Complex network theory [18], [19], [20] focuses on abstract network models such as "small-world" networks, which interpolate between regular lattices and random graphs, and scale-free networks, exhibiting a power law distribution of the connectivity. In most, if not all, of the theoretical work in contact network epidemiology, the host population contact network is represented by one of these models. The choice of the right idealized network type, which will be disease specific, depends on the availability of data on disease causing contacts which is hard to get and difficult to interpret [16]. At this point, an important concern of contact network epidemiology is to collect data and build appropriate network models for different transmission mechanisms [30].

As a first step to understanding the role of network structure correlations on the spectrum of stochastic fluctuations, we have modelled the mixing network of the populations as a small world network [21] built over a square lattice with 12 nearest neighbours per node. In these models a fraction of the links of the lattice is randomized by connecting nodes, with probability p , with any other node. These non-local connections are chosen randomly for each event, instead of being fixed in a frozen, partially random, link configuration. This version of the small world network model, which has been dubbed 'dynamic' or 'annealed' in the literature ([34], [35], [36]), is motivated by the nature of the occasional social contacts the model tries to represent. For $p = 0$, each node interacts only with its nearest neighbours on the lattice, as in ordinary representation of spatial structure. For $p = 1$, the network of interactions is a random graph, where every pair of nodes, independently of the distance on

the lattice between the two nodes, has the same probability of being connected. Random graphs have the property that the average path length, or average number of connections of the shortest path between two nodes, is 'small', i. e., of the order of the logarithm of the total number of nodes. For a range of p between 0 and 1 the network exhibits 'small world' behaviour, where predominantly local interactions (as in lattices) coexist with a short average path length (as in random graphs). Analysis of real networks [30] reveals the existence of small world behaviour in many interaction networks, including networks of social contacts.

An important consequence of the spatial correlations introduced by predominantly local contacts is what is called infective screening, or infective clustering. If all the infected neighbours of an infected node have many neighbours in common, each of them will be connected to a number of susceptibles which is smaller than the average number of susceptible neighbours per node, and infection will be less likely than in a randomly mixed population with the same density of infectious and of susceptibles.

The qualitative analysis of time series of SIR and SEIR stochastic simulations on dynamic small world networks for different values of the small world parameter p shows that indeed the infection process becomes less and less efficient as p decreases and infective screening becomes more pronounced [37], [38]. The global effect of infective clustering may be quantified in terms of the value of β_{eff} , defined as the average number of new infections per time step and infective individual divided by the density of susceptibles. For $p = 1$, β_{eff} coincides with the transmissibility β but, as p decreases, β_{eff} also decreases. Another qualitative effect of spatial correlations reported in [37], [38] is that they have a major effect on the enhancement of the amplitude of stochastic fluctuations, which become more and more pronounced as p decreases.

In order to quantify the effect of network structure on resonant stochastic fluctuations, we have computed the power spectrum of SIR time series on dynamic small world networks for several values of p , and we have compared it with the analytic power spectrum given by (3) with β_{eff} , the effective transmissibility, instead of β (see the Appendix for the details

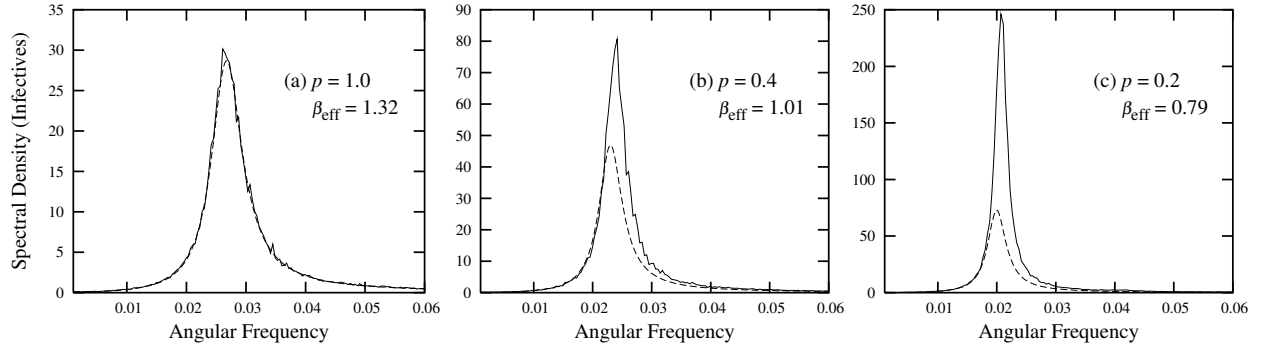


FIG. 1: Fluctuation power spectra of infectives time series for the SIR model on dynamic networks of $N = 10^6$ nodes for small world parameter p equal to (a) 1, (b) 0.4, and (c) 0.2; the networks are built over regular 1000×1000 lattices with 12 first neighbours and periodic boundary conditions. The full lines are the averaged numerical power spectra of 400 stationary time series, each 32768 timesteps long. The dashed lines are the analytic power spectra given by (3), where for p smaller than 1 the value of the parameter β has been taken as β_{eff} , defined as the actual number of new infections per time step and infective individual divided by the density of susceptibles. Parameter values: $\mu = 6 \times 10^{-4}$, $\beta = 1.32$, $\gamma = 1/8$.

of the simulations). The results are shown in Figure 1. The full lines are the averaged numerical power spectra of the stationary time series, and the dashed lines are the analytic power spectra given by (3) with the correction due to the effective transmissibility. We see that, as p decreases, the resonant fluctuations are larger and more coherent. Moreover, in the small world regime, where local correlations become important, this effect is much more pronounced than in the predictions of an effective (corrected for infective screening) randomly mixed model, represented by the dashed lines in Figure 1. However, this effective model does describe satisfactorily the shift to the left in the peak frequency, which means that this can be understood as a consequence of the reduced effective transmissibility.

The enhanced amplitude and coherence of the fluctuations implies that a typical time series will exhibit noisy but regular incidence oscillations, as shown in Section III.B. These sustained oscillations are of a purely stochastic nature, and they disappear in the infinite

population limit.

The influence of the recovery profile on the behaviour of the system has been discussed in [31], [33], [39]. In the standard SIR stochastic model, to which the analytic description (3) applies, the event of recovery occurs at a fixed rate during the infection, and the recovery time is exponentially distributed around the average infectious period $\tau = 1/\gamma$, or in other words uncorrelated. We have computed the power spectrum of the time series obtained from SIR simulations in randomly mixed populations where instead of uncorrelated infection periods the recovery profile was taken in the opposite limit of constant infection period τ or strongly time correlated infections. The results are shown in Figure 2. The full line is the averaged numerical power spectra of the stationary time series, and the dashed line is the analytic power spectra given by (3) with $\gamma = 1/\tau$. We see that switching to more realistic (time correlated) recovery profiles leads to a similar effect of enhancing the amplitude and the coherence of the resonant stochastic fluctuations predicted by the theory developed in [15]. In addition, there is a large shift to the right of the dominant frequency of the fluctuations, relative to the peak frequency predicted for the model with stochastic recovery [15]. Again, the shift in the peak frequency and its sign can be understood in terms of an effective deterministic description, as discussed in Section III.C.

Qualitatively, it is to be expected that correlations in the dynamics of the system's components should enhance the global density fluctuations. To assess quantitatively the effect of spatial and temporal correlations on the resonant fluctuations spectrum in the modelling of infectious childhood diseases, we have performed systematic simulations in a region of parameter space that includes the values for measles, chicken pox, rubella, pertussis and mumps according to published and estimated data for the pre-vaccination period [6]. The amplitude and coherence of the stochastic fluctuations are measured by the overall amplification A , and by the coherence factor c , introduced in [15], where analytic results for a randomly mixed SIR stochastic model with external infection and constant recovery rate were presented for the same region of parameter space. The overall amplification A is the integral over all the frequencies of the power density of the scaled fluctuations, and it is

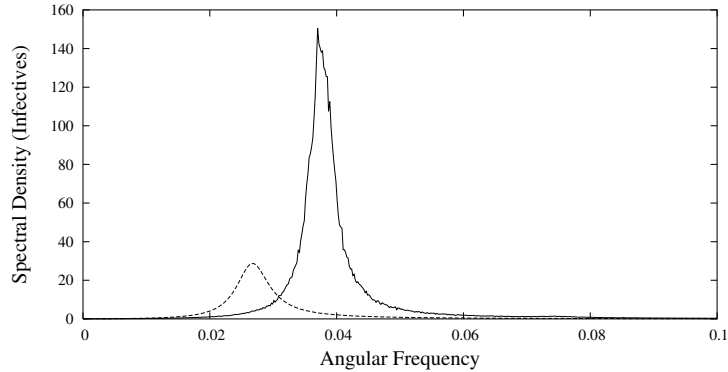


FIG. 2: Fluctuation power spectra of infectives time series of stochastic SIR dynamics with deterministic and stochastic recovery on a randomly mixed population with $N = 10^6$ individuals. Deterministic recovery occurs τ timesteps after infection. The full line is the averaged numerical power spectra of 400 stationary time series, each 32768 timesteps long. The dashed line is the analytic power spectra given by (3), with $\gamma = 1/\tau$. Parameter values: $\mu = 6 \times 10^{-4}$, $\beta = 1.32$, $\tau = 8$.

equal to the mean square deviation of the time series from the equilibrium values, divided by the system size N . The coherence factor c is defined as the integral of the power density of the scaled fluctuations on the frequency interval that corresponds to periods within 10% of the peak period $2\pi/\omega_{peak}$, divided by A . It measures the relative contribution to the overall amplification of stochastic fluctuations that are distributed around the dominant period.

For the randomly mixed case $p = 1$ with stochastic recovery, both A and c can be computed analytically from equations (3), which are exact in the limit of large N . In the remaining cases there is no analytic description, and the overall amplification A is computed as the ensemble average, over several runs, of the integral over all sampled frequencies of the power density of the stationary time series of the scaled fluctuations. The coherence factor c is computed in a similar way on the prescribed frequency interval. The details of the analytical and numerical computations are given in the Appendix.

For the model with stochastic recovery, we have also computed, for several values of the

small world parameter p , the peak shift factor s , defined as the distance between the actual peak frequency and the natural frequency of the system in the deterministic description (1), \sqrt{D} , divided by \sqrt{D} . It measures the relative frequency shift of the dominant frequency due to the various ingredients that are missing in the deterministic description (resonance with correlated internal noise, and contact network structure).

III. RESULTS

A. Randomly mixed model: finite size effects

The randomly mixed model depends on the demographic and epidemiological parameters μ , β and γ . Following [15], we have taken μ fixed and equal to 5.5×10^{-5} , and we have taken the reduced variables in the parameter plane $(\mu/\gamma, \beta/\gamma)$. These reduced parameters have an immediate epidemiological interpretation, μ/γ measures the acuteness, or relative time scale, of the disease, and $\beta/\gamma \approx R_0$.

The values of the overall amplification

$$A = \frac{1}{\pi} \int_0^{+\infty} P_I(\omega) d\omega \quad (4)$$

and of the coherence

$$c = \frac{1}{\pi A} \int_{\omega_{peak}/1.1}^{\omega_{peak}/0.9} P_I(\omega) d\omega \quad (5)$$

of the infectives power spectrum P_I in (3) are shown in Figure 3.(a) and 3.(b) for 441 points in parameter space. The values of A are normalized by the largest overall amplification 0.1902. We see that, for the basic SIR model, A is essentially determined by R_0 , and that both the overall amplification and the coherence increase as R_0 decreases with γ fixed. For each R_0 the stochastic oscillations become more and more coherent as γ increases. The symbols mark the parameter values for measles, chicken pox, rubella and pertussis according to different data sources for the pre-vaccination period [6]. The numerical results for the overall amplification and coherence obtained from simulations of the stochastic process (2) on a population of size $N = 10^6$ are plotted in Figures 3.(c) and 3.(d) (see the Appendix for

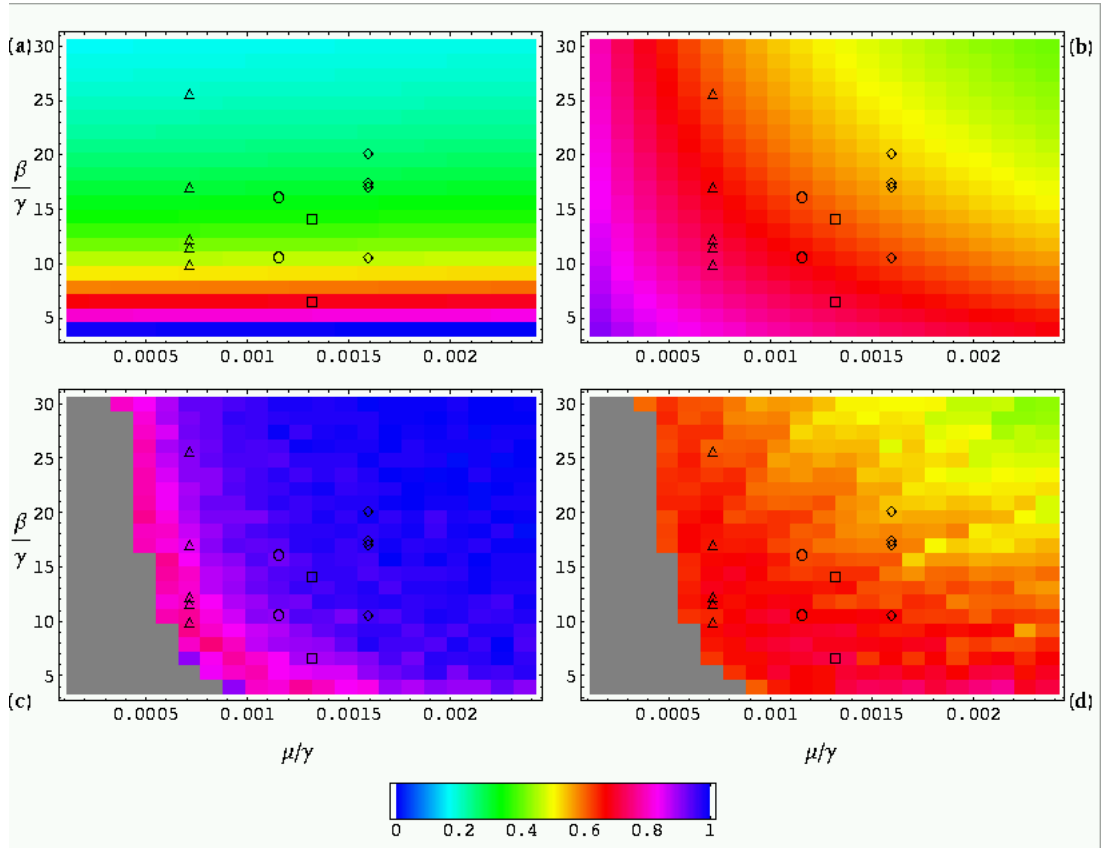


FIG. 3: Overall amplification and coherence of the randomly mixed model with stochastic recovery for 21×21 points in parameter space. The symbols mark the parameter values for measles (triangles), chicken pox (circles), rubella (squares) and pertussis (diamonds) according to different data sources for the pre-vaccination period. Analytic results for the amplification A in (a), and for the coherence c in (b). The values of (a) are normalized by the largest overall amplification 0.1902. In (c) and (d) are plotted the numerical results for the overall amplification and coherence obtained from simulations of the stochastic process (2) on a population of size $N = 10^6$. Shown in (c) are the values of the analytic plot (a) divided by the corresponding numerical values. Grey areas denote regions of parameter space for which less than 200 surviving runs 2^{15} timesteps long were obtained out of 500 trials.

the details of the simulations and numerical computations). Each data point in Figure 3.(c) is the ratio of the corresponding analytic and numerical values of the overall amplification, while each data point in Figure 3.(d) corresponds to the numerical value of the coherence as defined in (5). The data points shown in grey correspond to parameter values where more than 60% of the 50 000 days long simulations ended up with zero infectives. It is clear that for realistic population sizes, in a large region of parameter space, there are corrections to the analytic results of Figure 3.(a) and 3.(b), and that the fluctuations for small β and large γ are larger than those predicted by the analytic approach. The numerical power spectra obtained from stochastic simulations for $N = 10^6$ and $N = 50 \times 10^6$ for values of $(\mu/\gamma, \beta/\gamma)$ for which these corrections are more significant are shown in Figure 4.(a). The analytic power spectrum given by (3) overlaps the numerical curve for $N = 50 \times 10^6$ within the resolution of the figure. A breakdown of the analytic description for $N = 10^6$ can be detected in the overall amplification and in the peak frequency shift, as well as in the loss of coherence due to the appearance of a small harmonic peak. This effect is more pronounced in the presence of spatial correlations, as shown in Figure 4.(b) and discussed in the following section.

The limitations of the analytic description (3) are due to the fact that a linear theory based on van Kampen's method is used to approximate the master equation up to next to leading order terms, leaving out the contribution of terms of order $1/\sqrt{N}$ and higher, whose influence on the dynamics becomes more important as the system size and/or the stability of the stationary state decreases.

B. Small world network: effects of spatial correlations

To assess the effect of spatial correlations on the resonant fluctuations spectrum, we have performed, for the same 441 points in parameter space, systematic simulations of SIR time series on dynamic small world networks for several values of p (see the Appendix for the details of the simulations). The results for the overall amplification A when $p = 0.6$ are shown in Figure 5.a). The values of A are normalized by the largest value of the

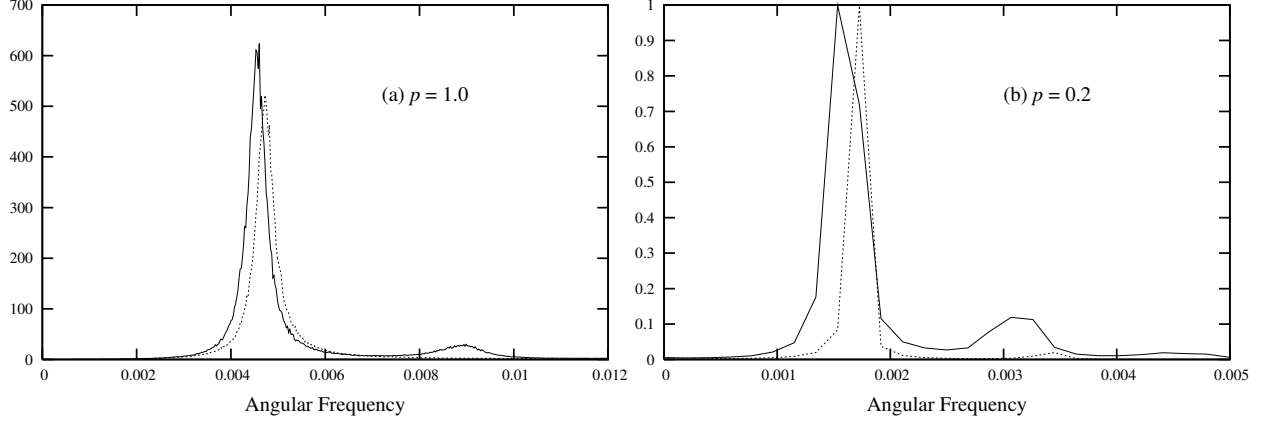


FIG. 4: (a) Numerical power spectra obtained from stochastic simulations for $N = 10^6$ and $N = 50 \times 10^6$ (full and dotted lines, respectively) for values of $(\mu/\gamma, \beta/\gamma) = (0.00094, 7.9)$. The spectra were taken from 2^{18} , instead of 2^{15} , timesteps long simulations for increased resolution in frequency. The curve for $N = 10^6$ shows a larger overall amplification and a peak frequency shift, as well as loss of coherence due to the appearance of a small harmonic peak. (b) Power spectra of stochastic simulations on a dynamic small world network with $p = 0.2$ and $N = 10^6$ nodes (full line) and $N = 50 \times 10^6$ (dotted line), for the parameter values $(\mu/\gamma, \beta/\gamma) = (0.00182, 4.0)$ chosen in the region where the amplitude of the harmonic peaks is larger. Both plots are scaled to the largest spectral power (3960 for $N = 10^6$ and 71000 for $N = 50 \times 10^6$). The ratio of the heights of the 2nd peak to the 1st peak is approximately $7 \approx \sqrt{50}$ times smaller for the larger system, in line with the expected $1/\sqrt{N}$ dependence.

overall amplification, which is 0.2908. With respect to the analytic spectrum (3), the overall amplitude of the fluctuations increases by a factor of about 1.5, causing more occasional extinctions. As before, the grey region corresponds to parameter values where more than 60% of the 50 000 days long simulations ended up with zero infectives. The dependence of the amplitude of the fluctuations on the epidemiological parameters is qualitatively the same as for the randomly mixed ($p = 1$) numerical results of Figure 3.(c). It increases as R_0 decreases, and, for fixed R_0 , it increases as γ increases. Close to the extinction boundary, especially for low R_0 we find a departure from this general trend which can be

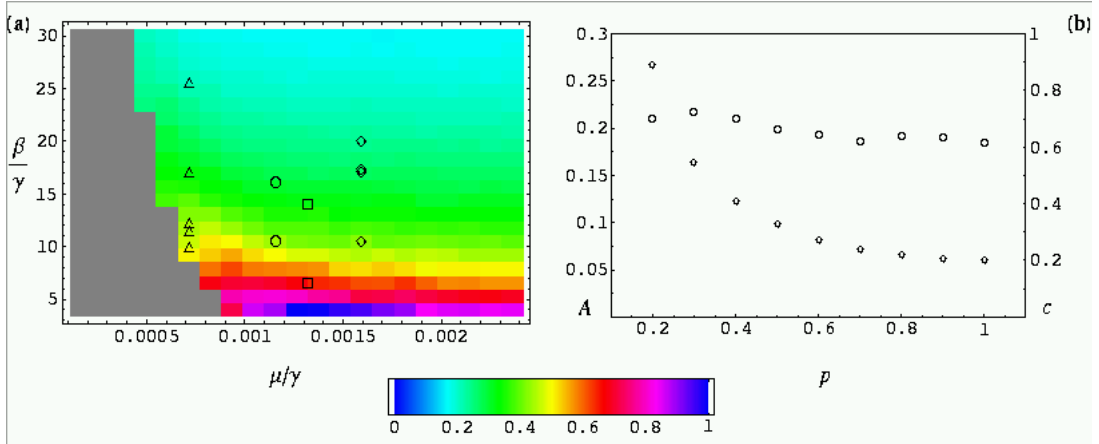


FIG. 5: (a) Overall amplification of the SIR model with stochastic recovery on a dynamic small world network with $N = 10^6$ individuals and $p = 0.6$ (see the Appendix for details of the simulations). The values of the overall amplification A are normalized in the plot by the largest amplitude (0.2908). Again, grey areas denote regions where only a small percentage of timeseries survive after 2^{15} timesteps (each sampled point requires the survival of at least 200 out of 500 runs). (b) Amplification A (diamonds) and coherence c (circles) for the point $(\mu/\gamma, \beta/\gamma) = (0.00116, 17.0)$ as a function of the small world parameter p . The chosen point lies approximately at the center of the region plotted in (a).

due a sampling bias, as we have had to select long time series without disease extinction from a large ensemble of trial runs.

The most relevant effect of spatial correlations is the increase in the amplitude of the fluctuations as the small world parameter p decreases. The plot of the overall amplification A as a function of p is shown in Figure 5.b) (data points plotted with diamonds) for parameter values close to those of pertussis (for other disease parameter values the behaviour of the amplitude of the fluctuations as a function of p is similar). There is a four-fold increase in the amplitude of the fluctuations for $p = 0.2$ with respect to the randomly mixed case $p = 1$.

For the same parameter values, the plot of the coherence c as a function of p is also shown in Figure 5.b) (data points plotted with circles). There is an increase in the coherence of the

fluctuations as p decreases, which means that as the fluctuations get larger they also exhibit a more regular temporal pattern. For a fixed value of p , the coherence is uniformly very high in parameter space (results not shown), with changes of less than 10% in a region that includes all the parameter values considered for childhood infectious diseases. However, in a small region close to the $\beta/\gamma = 4$ horizontal line and for $p = 0.2$ there is loss of coherence, due to the appearance of harmonic peaks, see Figure 4.(b), which are more pronounced than the ones found for $p = 1$, and persist for larger values of N . Although the relative amplitude of the harmonic peaks seems to scale with $1/\sqrt{N}$, the fact that they are enhanced is due to the presence of spatial correlations, and could be related to the existence of an oscillatory phase for small values of μ/γ in deterministic SIR models that include, at the simplest level, the effect of these correlations [40]. Indeed, the breakdown of Van Kampen's $1/\sqrt{N}$ scaling is expected in the oscillatory phase of this model, where the ratio of the amplitudes of the harmonic peaks is constant, in the infinite size limit.

The combined effect of the spatial correlations on the amplitude and on the coherence of the fluctuations can be seen in Figure 6, where a typical time series for the parameter values of Figure 5.(b) and $p = 0.2$ is shown. The purely stochastic incidence peaks can be as high as 3500 individuals per day in a population of $N = 10^6$, with troughs of one or two hundred infectious, and a period of recurrence of epidemics can be clearly identified. Indeed, the pattern of sustained oscillations shown in Figure 6 is similar to that found in incidence data for measles in the prevaccination records of english cities of comparable population size [41], and it is more sharply defined than that of real time series for most childhood diseases incidence data [42], [43], [44], [45].

Another important effect of contact network structure is the shift in the dominant frequency of the power spectrum. In Figure 7 we plot, as a function of p , the peak shift factor s , defined as the difference between the actual peak frequency and the natural frequency of the system in the deterministic description (1), \sqrt{D} , divided by \sqrt{D} . Again, we have chosen the same parameter values of Figure 5.b), $(\mu/\gamma, \beta/\gamma) = (0.00116, 17.0)$, but the results for other points in parameter space are similar. We found that, as p decreases, the dominant

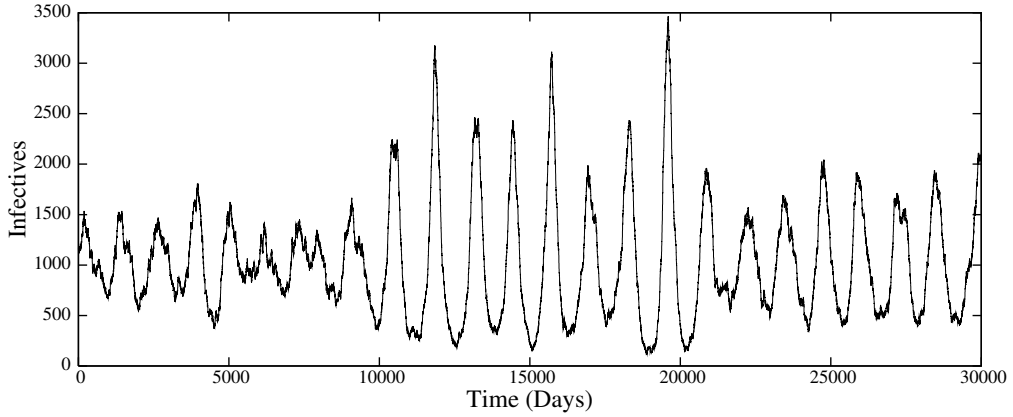


FIG. 6: Typical incidence time series for a population of $N = 10^6$ and small world parameter $p = 0.2$. We have taken $(\mu/\gamma, \beta/\gamma) = (0.00116, 17.0)$ as in Figure 5.b).

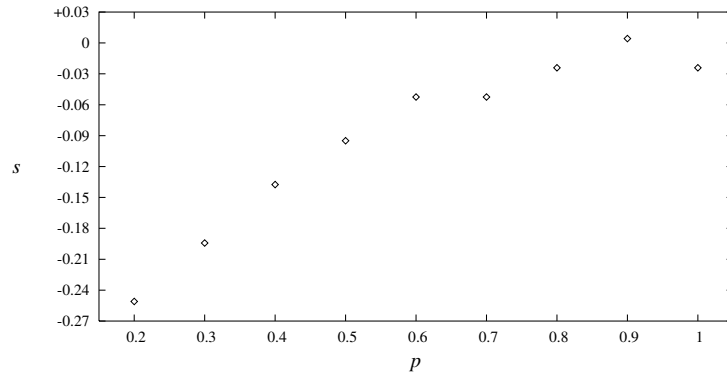


FIG. 7: The peak shift factor s as a function of the small world parameter p . We have chosen $(\mu/\gamma, \beta/\gamma) = (0.00116, 17.0)$, the same parameter values as in Figure 5.(b).

frequency of the time series is shifted increasingly to the left. As discussed in Section II, this can be understood as a result of the reduced effective transmissibility due to clustering of infectives. Since both the overall amplification and the coherence increase as p decreases, the time series of long term simulations will, as shown in Figure 6, exhibit recurrent epidemics with approximate period close to that given by the dominant frequency of the resonant fluctuations. However, this value can be very different from the period that corresponds to

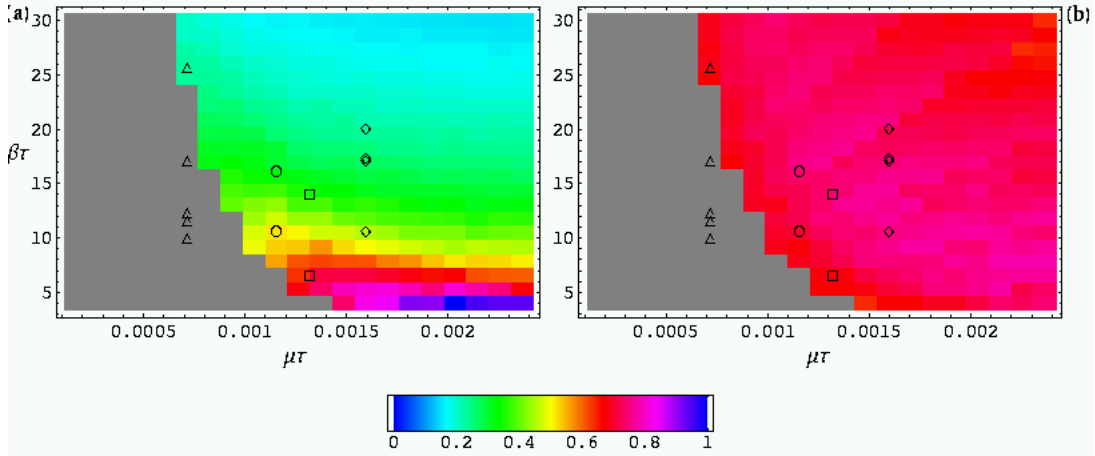


FIG. 8: Overall amplification (a) and coherence (b) for the randomly mixed SIR model with deterministic recovery over a population of $N = 10^6$ individuals. The values of (a) are normalized by the largest overall amplification 0.6901. Again, grey areas denote regions of parameter space where less than 200 out of 500 runs survive 2^{15} timesteps.

the natural frequency of the system in the deterministic limit (1).

C. Recovery profile: effects of time correlations

The results for the overall amplification and coherence in the the randomly mixed SIR model with deterministic recovery are shown in Figure 8. The values of A in Figure 8.(a) are normalized by the largest value of the overall amplification 0.6901, which means that the overall amplitude of the fluctuations increases by a factor of about 3.5 with respect to the model with stochastic recovery. In agreement with the results of Figure 2, the enhancement of the peak amplitude will in general be even larger, since, as shown in Figure 8.(b), the coherence of the fluctuations for the case of deterministic recovery is larger for most parameter values. Realistic recovery profiles will therefore be associated with time series whose fluctuations power spectra will be larger and more sharply peaked than for constant recovery rate models. The peak frequency shift relative to this model is towards larger frequencies, and it may partially cancel the effect of internal noise correlations that shifts the peak frequency

to the left of \sqrt{D} , bringing the resulting dominant frequency closer to the natural frequency of the system in the deterministic description.

In [39], the basic SIR model (1) was modified to include a family, parametrized by an integer n , of infectious periods distributions that interpolate between the exponential distribution (for $n = 0$) and delta distribution associated to deterministic recovery (in the limit $n \rightarrow \infty$). Although there is no simple expression in closed form in this case for the period of the damped oscillations close to the system's equilibrium, it was shown that the period decreases as n increases. Our findings are in agreement with the expectation of an increase of the dominant frequency in the limit of fixed recovery time.

IV. DISCUSSION AND CONCLUSIONS

The relevance of the phenomenon of resonance with internal noise for the understanding of the long term dynamics of childhood infections, with or without the presence of seasonal forcing, has been uncovered in [15]. The power spectrum of the fluctuations of the stochastic process of infection in a population has been given a complete analytic description, under the following basic assumptions:

1. There is external infection at a small constant rate
2. The population is randomly mixed and internal infection follows a law of mass-action with constant transmissibility
3. Recovery from the disease occurs at a constant rate
4. The behavior of the fluctuations is well described by the lowest order van Kampen expansion of the master equation,

that correspond to a stochastic open SIR model and large population sizes.

We have extended the analytic results of [15] to a closed stochastic SIR model, with no external infection, that models an isolated population, and compared these with the results of extensive numerical simulations. Due to stochastic extinctions, simulations of the long term behaviour of this model require large population sizes, and we took $N = 10^6$ as a typical value for the population size. We have found a good agreement between the analytic

description and the results of the simulations for most values of the parameters. However, in a region of parameter space that includes in particular measles, we have found that there are significant finite size corrections to the analytic power spectrum of the fluctuations, which means that assumption 4 is fulfilled only for much larger population sizes (indeed for population sizes of $N = 5 \times 10^7$ we have found good agreement between the analytic description and the results of the simulations, over the whole range of parameters).

We have then investigated the effects on the fluctuation power spectrum of relaxing 2 or 3 in order to account for more realistic contact networks of the population or disease recovery profiles. These are examples spatial and temporal correlations that are always present in real interacting systems. In either case, the approximate analytic description is no longer valid, and we must resort to systematic simulations. However, we have found fluctuation power spectra that are dominantly resonant like, which suggests that the basic mechanism at play is still resonance with demographic stochasticity.

Instead of assuming 2, we have modelled the mixing network of the populations as a dynamic small world network, and considered several different values of the small world parameter p that measures the degree of randomness of the contact network. We have found that, as p decreases, the resonant fluctuations become larger and more coherent over the whole range of parameters that are relevant for the description of childhood infections, and the dominant frequency of these fluctuations is shifted towards smaller frequencies.

Instead of 3, we have considered the opposite (strongly correlated) limit of deterministic recovery at the end of the infectious period. Clearly, realistic recovery profiles will lie between these two extremes. We have found, again, resonant fluctuations that are much larger, and more coherent than when recovery occurs randomly at a constant rate, and that the dominant frequency is shifted to larger frequencies.

The main conclusion is then that the importance of the phenomenon reported in [15] to the description of the long term dynamics of childhood diseases is enhanced when the model is modified to include more realistic assumptions (correlations), either on the populations contact patterns (spatial correlations) or on the disease recovery profile (time correlations).

Our results apply to a large region in the epidemiological and demographic parameter space, and in this sense they are applicable in general to the modelling of infectious disease dynamics. They show that stochasticity may play the leading role in determining the incidence temporal patterns, through resonance of internal noise with the dynamics that governs the system in the limit of an infinite population.

Our results also show that the analytic theory developed in [15] provides an overall good description for well mixed populations and diseases with gradually decaying recovery profiles, and a useful guideline for the case of populations with non trivial contact networks. When these contact networks include a large fraction, of 50% or more, of random connections, an effective theory based on the analytic treatment of the randomly mixed case with a correction of the transmissibility to account for infective screening gives a good description of the incidence fluctuations spectrum. In highly correlated contact networks, however, the overall amplitude of the fluctuations is much larger than that predicted by this effective theory.

The qualitative picture for the dependence of demographic stochasticity on the system parameters that emerges from our results is more subtle than what one would expect from linear perturbation analysis, either of the deterministic model (1) or even of the full stochastic description (2). First, in the presence of correlations, the dominant frequency of these resonant organized fluctuations differs significantly from the natural frequency of the deterministic description. The fact that this naive expectation may seem to lead to a good description, as argued in [6], must be attributed to the cancelation of several missing effects. Second, the amplitude of these fluctuations decreases with N , or more precisely with \sqrt{N} , but finite size effects will be important for realistic population sizes, of the order of 10^6 , except for diseases with an epidemiological profile similar to that of pertussis. Third, the amplitude of the fluctuations increases when R_0 decreases, and, for fixed R_0 , it decreases as γ decreases. This additional dependence of the amplitude of the fluctuations on the average infectious period is unaccounted for by the analytic description (3).

On more conceptual grounds, the finding that in finite, discrete populations internal noise

together with correlations produces sustained incidence oscillations of significant amplitude all over the parameter region that includes childhood infectious diseases is of importance for the long-standing controversy in epidemiology and ecology as to the driving mechanisms of the pervasive noisy oscillations observed in these systems [46]. Whether these are mainly intrinsic or external seems to depend not only on the model's nonlinearities but also on the correlations between the systems's units, which most traditional approaches neglect.

As the need for spatial models of infectious disease transmission is increasingly acknowledged, there are different modelling strategies that try to reconcile explicit spatial representation with computational costs and the information available on the patterns of contact of the populations (see [47] and references therein). In the context of this discussion, it should be stressed that the kind of intrinsic stochastic effects highlighted in the present paper is specific of models that explicitly represent individuals (or small units such as households), and that computationally lighter, coarse-grained models will miss this phenomenology.

V. APPENDIX

All simulations were carried out over a population of individuals arranged on a square lattice with periodic boundaries where each site connects to its 12 closest neighbours. A random fraction p of these local links are replaced at each step with random long-distance links. The population size was 10^6 individuals for all simulations, with the exception of the results of Figure 4 where a population of 50×10^6 individuals was also considered.

The simulations implemented the stochastic process of the SIR model, or its modification to include deterministic, instead of stochastic, recovery, on this network. For the case of stochastic recovery, we have used the efficient algorithm for stochastic processes in spatially structured systems described in [48]. Local and long range infections are dealt with separately, and a local (resp. long range) infection event occurs with probability $1 - p$ (resp. p). For $p = 1$, the presence of spatial structure is irrelevant, and the algorithm reduces to the application of the method of Gillespie [49] to the stochastic process (2). When $p < 1$ and local infections may occur, their probability depends on the number of infected neighbours

of each susceptible node, and so susceptible nodes with k infected neighbours, $k = 0, \dots, 12$ are treated as separate classes. For the case of stochastic recovery, this algorithm is extended with the inclusion of a linked list of infected nodes. Each entry in the list records the position of an infected node in the lattice, along with the timestep number (counting from 0 at the start of the run) at which this particular node should recover (in case it has not been removed previously by a stochastic death transition). The list is ordered by recovery timestep number; that is, it always contains the oldest nodes at the start. In this way, recovery is efficiently performed by checking, at the beginning of each timestep, which nodes are due for recovery and replacing them in the lattice with recovered nodes

The numerical results of Figures 3, 5 and 8 were obtained through systematic simulations of the SIR model for a set of 21×21 evenly spaced points covering the $(\mu/\gamma, \beta/\gamma)$ plane, for the region depicted in the figures (and keeping $\mu = 5.5 \times 10^{-5}$ fixed). Four separate sets of simulations were carried out, one for each of the specific cases considered in the main text, namely, the SIR model with stochastic recovery for $p = 1.0$ and for $p = 0.6$, the SIR model with stochastic recovery for $(\mu/\gamma, \beta/\gamma) = (0.00116, 17.0)$ and several values of p , and the SIR model with deterministic recovery and $p = 1.0$.

For each sample point, 500 independent runs of the model were taken, each lasting for 50000 timesteps or days, of which only the last 2^{15} are used; approximately 17000 timesteps are discarded at the beginning, to allow each run to ‘settle down’ to its steady state. If less than 200 of these 500 runs survive (that is, finish with more than zero infectives), then this particular sample point is discarded (shown as grey in the plots); otherwise, the power spectral densities of the surviving runs are computed (using an FFT routine) and averaged together. The remaining power spectrum plots shown in the Figures were obtained in the same way, except those of Figure 4.(a), in which 2^{18} timesteps long stationary timeseries were used, 8 times longer than those used for other plots, to provide the increased frequency resolution necessary to check the perfect agreement with the the analytical prediction (3) for 50×10^6 individuals.

From the final averaged spectrum, the quantities A , c and s are computed. The overall

amplification, which is defined as $A = \frac{1}{\pi} \int_0^{+\infty} P_I(\omega) d\omega$, where $P_I(\omega)$ is the power spectrum density of the scaled fluctuations, is numerically approximated by a sum over the squared moduli of the scaled coefficients Z_k/\sqrt{N} of the discrete Fourier transform of the timeseries. Since the sampling interval is 1 day, the band width of the signal is $\omega \in [-\pi, \pi]$, and we have

$$A \approx \frac{1}{\pi} \int_0^{+\pi} P(\omega) d\omega = \frac{1}{L} \int_0^L P(\pi k/L) dk \approx \frac{1}{L} \sum_{k=0}^{L-1} \frac{|Z_k|^2}{N}$$

where k is the integer index of the Fourier coefficient and L the sample length (here $L = 2^{15}$). The coherence is defined as $c = A_p/A$, where A_p is the integral of the power spectrum density of the scaled fluctuations over the frequency range that corresponds to $\pm 10\%$ of the period of the dominant peak. The numerical value of A_p is obtained in the same manner as A from the squared moduli of the scaled coefficients Z_k/\sqrt{N} , replacing the summation limits appropriately.

The position of the dominant peak ω_{peak} is found from the largest Fourier coefficient, and is also used to compute the shift factor $s = (\omega_{peak} - \sqrt{D})/\sqrt{D}$ shown in Figure 7.

VI. ACKNOWLEDGEMENTS

Financial support from the Foundation of the University of Lisbon and the Portuguese Foundation for Science and Technology (FCT) under contracts POCI/FIS/55592/2004 and POCTI/ISFL/2/618 is gratefully acknowledged.

-
- [1] R. A. Anderson and R. M. May, *Infectious Diseases of Humans*, Oxford U. P., Oxford, 1991.
 - [2] H. W. Hethcote, An age-structured model for pertussis transmission, *Math. Biosci.***145**, 89-136 (1997)
 - [3] B. T. Grenfell, O. N. Bjørnstad and J. Kappey, Travelling waves and spatial hierarchies in measles epidemics, *Nature* **414**, 716-723 (2001)

- [4] W. Wang, Epidemic models with nonlinear infection forces, *Math. Biosci. & Eng.* **3**, 267-279 (2006)
- [5] D. J. D. Earn, P. Rohani, B. M. Bolker and B. T. Grenfell, A Simple Model for Complex Dynamical Transitions in Epidemics, *Science* **287**, 667-670 (2000)
- [6] C. T. Bausch and D. J. D. Earn, Transients and attractors in epidemics, *Proc. R. Soc. Lond. B* **270**, 1573-1578 (2003)
- [7] J. Dushoff, J. B. Plotkin, S. A. Levin and D.J.D. Earn, Dynamical resonance can account for seasonality of influenza epidemics, *Proc. Nat. Acad. Sci.* **101**, 16915-16916 (2004)
- [8] M. S. Bartlett, Measles periodicity and community size, *J. R. Stat. Soc. A* **120**, 48-70 (1957)
- [9] I. Nåsell, A new look at the critical community size for childhood infections, *Theor. Pop. Biol.* **67**, 203-216 (2005)
- [10] N. T. J. Bailey, *The Mathematical Theory of Infectious Diseases*, 2nd edition, Charles Griffin & Co, London, 1975
- [11] A. L. Lloyd, Estimating variability in models for recurrent epidemics: assessing the use of momentum closure techniques, *Theor. Pop. Biol.* **65**, 49-65 (2004)
- [12] M. J. Keeling, P. Rohani and B. T. Grenfell, Seasonally forced disease dynamics explored as a switching between attractors, *Physica D* **148**, 317-335 (2001)
- [13] L. J. S. Allen and P. van den Driessche, Stochastic epidemic models with a backward bifurcation, *Math. Biosci. & Eng.* **3**, 445-458 (2006)
- [14] A. J. McKane and T. J. Newman, Predator-Prey Cycles from Resonant Amplification of Demographic Stochasticity, *Phys. Rev. Lett.* **94**, 218102 (2005)
- [15] D. Alonso, A. J. McKane and M. Pascual, Stochastic amplification in epidemics, *J. R. Soc. Interface* DOI:10.1098/rsif.2006.0192 (2006)
- [16] M. J. Keeling and K. T. D. Eames, Networks and Epidemic Models, *J. R. Soc. Interface* **2**, 295-307 (2005)
- [17] W.J. Edmunds, G. Kafatos, J. Wallinga and J. Mossong, Mixing patterns and the spread of close-contact infectious diseases, *Emerging Themes in Epidemiology* **3**, 10 (2006)
- [18] R. Albert, A.-L. Barabasi, Statistical mechanics of complex networks, *Rev. Mod. Phys.*, **74**, 47

(2002)

- [19] S.N. Dorogovtsev and J.F.F. Mendes, *Evolution of networks*, Oxford U. P., 2003
- [20] S. Boccaletti, V. Latora, Y. Moreno, M. Chavez, D.-U. Hwang, *Complex networks: Structure and dynamics*, *Phys. Rep.* 424, 175-308 (2006)
- [21] D.J. Watts, S.H. Strogatz, *Collective dynamics of small-world networks*, *Nature*, 393, 440 (1998)
- [22] M. Kuperman, G. Abramson, *Small world effect in an epidemiological model*, *Phys. Rev. Lett.*, 86, 2909 (2001)
- [23] R. Pastor-Satorras, A. Vespignani, *Epidemic spreading in scale-free networks*, *Phys. Rev. Lett.*, 86, 3200 (2001)
- [24] R.M. May and A. Lloyd, *Infection dynamics on scale-free networks*, *Phys. Rev. E* 64, 066112 (2001)
- [25] K.T.D. Eames and M.J. Keeling, *Modelling dynamic and network heterogeneities in the spread of sexually transmitted diseases*, *Proc. Natl. Acad. Sci. USA* 99, 13330-13335 (2002)
- [26] M.J. Keeling, *Implications of network structure for epidemic dynamics*, *Theor. Popul. Biol.* 67, 1-8 (2005)
- [27] A.M. Jolly and J.L. Wylie, *Gonorrhoea and Chlamydia core groups and sexual networks in Manitoba*, *Sex. Transm. Infect.* 78, i45-i51 (2002)
- [28] S. Riley et al., *Transmission dynamics of the etiological agent of SARS in Hong-Kong: impact of public health interventions*, *Science* 300, 1961 - 1966 (2003)
- [29] L. A. Meyers, B. Pourbohloul, M.E.J. Newman, D.M. Skowronski and R.C. Brunham, *Network Theory and SARS: predicting outbreak diversity*, *J. Theor. Biol* 232, 71-81 (2005)
- [30] S. Eubank, H. Guclu, V. S. Anil Kumar, M. V. Marathe, A. Srinivasan, Z. Torockzcai and N. Wang, *Modelling disease outbreak in realistic urban social networks*, *Nature* **429**, 180 (2004).
- [31] M.J. Keeling and B. T. Grenfell, *Disease Extinction and Community Size: Modeling the Persistence of Measles*, *Science* **275**, 65-67 (1997)
- [32] A. L. Lloyd, *Realistic Distributions of Infectious Periods in Epidemic Models: Changing Patterns of Persistence and Dynamics*, *Theor. Pop. Biol.* **60**, 59-71 (2001)

- [33] H. J. Wearing, P. Rohani and M. J. Keeling, Appropriate Models for the Management of Infectious Diseases, *PLoS Med.* **2**, e174 (2005)
- [34] D. Zanette D, Dynamics of rumor propagation on small-world networks, *Physical Review E* **65**, 041908 (2003)
- [35] G. Szabo and J. Vukov, Cooperation for volunteering and partially random partnerships, *Phys. Rev. E* **69**, 036107 (2004)
- [36] E Volz and L A Meyers, SIR epidemics in dynamic contact networks, arXiv:0705.2105
- [37] J. Verdasca, M. M. Telo da Gama, A. Nunes, N. R. Bernardino, J. M. Pacheco and M. C. Gomes, Recurrent epidemics in small world networks, *J. Theor. Biol.* **233**, 553 (2005)
- [38] M. M. Telo da Gama and A. Nunes, Epidemics in small world networks, *European Physical Journal B - Condensed Matter* **50**, 205-208 (2006)
- [39] A. L. Lloyd, Destabilization of epidemic models with the inclusion of realistic distributions of infectious periods, *Proc. R. Soc. Lond. B* **268**, 985-993 (2001)
- [40] J. Benoit, A. Nunes and M. M. Telo da Gama, Pair approximation models for disease spread, *European Physical Journal B - Condensed Matter* **50**, 177-181 (2006)
- [41] www.zoo.ufl.edu/bolker/measdata.htm
- [42] L. F. Olsen, G. L. Truty and W. M. Schaffer, Oscillations and Chaos in Epidemics: A Nonlinear Study of Six Childhood Diseases in Copenhagen, Denmark, *Theor. Pop. Biol.* **33**, 344-370 (1988)
- [43] N. M. Ferguson, R. M. Anderson and G. P. Garnett, Mass vaccination to control chickenpox: the influence of zoster, *Proc. Nat. Acad. Sci.* **93**, 7231-7235 (1996)
- [44] H. Broutin, J.-F. Guégan, E. Elguero, F. Simondon and B. Cazelles, Large-Scale Comparative analysis of Pertussis Populations Dynamics: Periodicity, Synchrony and Impact of Vaccination, *Am. J. Epidemiology* **161**, 1159-1167 (2005)
- [45] H. Trottier, P. Philippe and R. Roy, Stochastic modelling of empirical time series of childhood infectious disease data before and after mass vaccination, *Emerging Themes in Epidemiology* **3:9** (2006), available from www.ete-online.com/content/3/1/9
- [46] B. Grenfell and O. Bjørnstad, Epidemic cycling and immunity, *Nature* **433**, 366 (2005).

- [47] S. Riley, Large-Scale Spatial Transmission Models of Infectious Disease, *Science* **316**, 1298-1301 (2007)
- [48] A. B. Bortz, M. H. Kalos and J. L. Lebowitz, A new algorithm for Monte Carlo simulation of Ising spin systems, *Journal of Computational Physics* **17**, 10 (1975)
- [49] D. T. Gillespie, A general method for numerically simulating the stochastic time evolution of coupled chemical reactions *J. Comput. Phys.* 22, 403 (1976)